Electronic Supplementary Information

Non-linear optical response by functionalized gold nanospheres: identifying design principles to maximize the molecular photo-release

Luca Bergamini[1,2,3,4], Valerio Voliani[5,6], Valentina Cappello[5], Riccardo Nifosì[7,6] and Stefano Corni[1]

1. Centro S3, CNR Istituto Nanoscienze, Modena, Italy
2. Dipartimento di Scienze Fisiche, Informatiche e Matematiche, Università di Modena e Reggio Emilia, Modena, Italy
3. Department of Electricity and Electronics, Faculty of Science and Technology, UPV/EHU, Bilbao, Spain
4. Materials Physics Center CSIC-UPV/EHU and Donostia International Physics Center DIPC, Donostia-San Sebastian, Spain
5. Center for Nanotechnology Innovation@NEST, Istituto Italiano di Tecnologia, Pisa, Italy
6. NEST - Scuola Normale Superiore, Pisa, Italy
7. NEST, Istituto Nanoscienze-CNR, Pisa, Italy

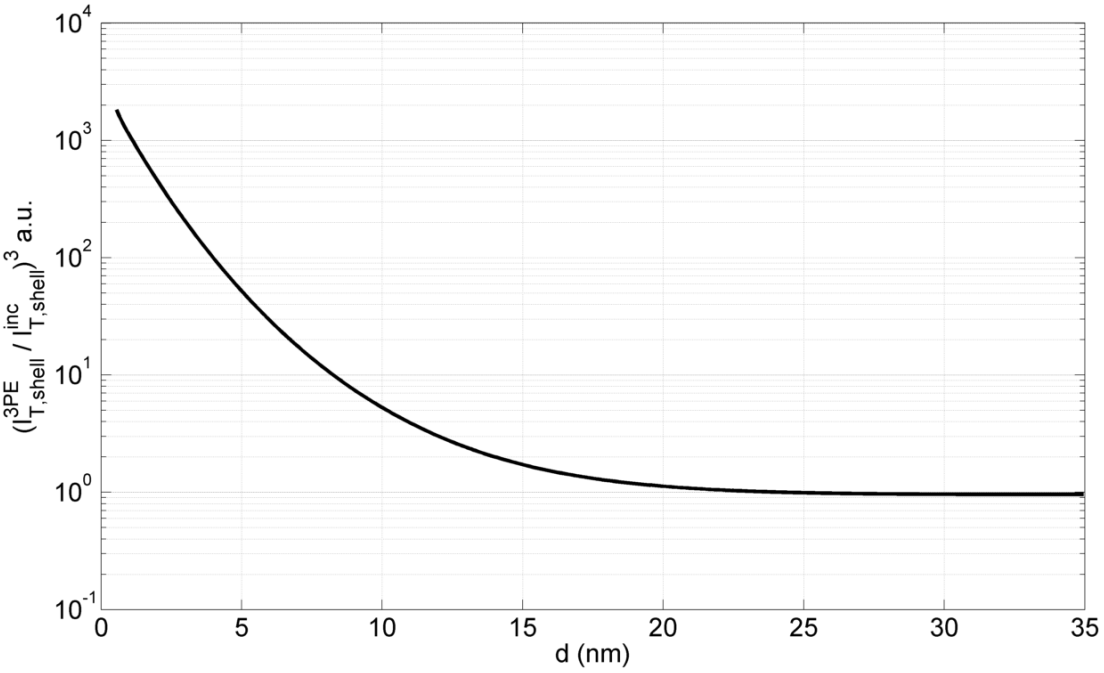

Figure S1 Third power of the shell- and time-averaged total electromagnetic field intensity as a function of the distance from the NP surface (d).

The quantity plotted in Figure S1 is the enhancement of the electromagnetic field intensity averaged over time and over a shell surrounding the nanoparticle ($I_{T,shell}$),

which is given by:

$$I_{T,shell} = I_{T,shell}(r) = \sqrt{\frac{\tilde{\varepsilon}}{\tilde{\mu}}} \langle \left| \vec{E}_{tot}(\vec{r},t) \right|^2 \rangle_{T,shell} \tag{S1}$$

$$= \sqrt{\frac{\tilde{\varepsilon}}{\tilde{\mu}}} \frac{\int_{\vec{r}}^{\vec{r}+\Delta\vec{r}} \left[\frac{1}{T} \int_0^T \left| \vec{E}_{tot}(\vec{r},t) \right|^2 dt \right] sin(\beta(\vec{r}))\, d\vec{r}}{\int_{\vec{r}}^{\vec{r}+\Delta\vec{r}} sin(\beta(\vec{r}))\, d\vec{r}} \tag{S2}$$

$$\simeq \sqrt{\frac{\tilde{\varepsilon}}{\tilde{\mu}}} \frac{\sum_i^{\vec{r}\leq\vec{r}_i\leq\vec{r}+\Delta\vec{r}} \left[\frac{1}{T} \int_0^T \left| \vec{E}^i_{tot}(\vec{r}_i,t) \right|^2 dt \right] sin(\beta_i(\vec{r}_i))}{\sum_i^{\vec{r}\leq\vec{r}_i\leq\vec{r}+\Delta\vec{r}} sin(\beta_i(\vec{r}_i))} \tag{S3}$$

where β (β_i) is the angle between the (i^{th}) point position vector and the x-axis (see Figure S2), while dr is the shell thickness. We recall that in our calculations the incident radiation is represented by a plane wave propagating along the z-axis with a x-polarized electric field. Note that the average over the space, which generally involves an integral, is eventually carried out as a finite sum over the electric field values evaluated on a grid basis. The result of Figure S1 is plotted as a function of the distance from the NP surface $d = r - R = r - 15$nm. For the calculation to be performed we set-up a fine polar grid with r, θ, ϕ lying in the range 15.5nm$\div$30nm, $0^\circ \div 180^\circ$, $0^\circ \div 360^\circ$ and having a step of 0.05nm, 1°, 1°, respectively. The aim of such a grid is to include the same number of points where the electric field is evaluated in each shell required for the calculation of the shell-average.

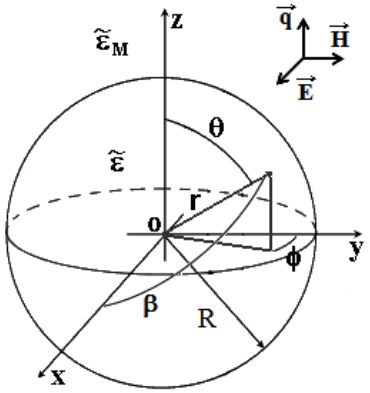

Figure S2 Sketch of the nanoparticle model. The wave vector of the incident radiation is set to be along the z-axis, whereas the incident electric filed is along the x-axis

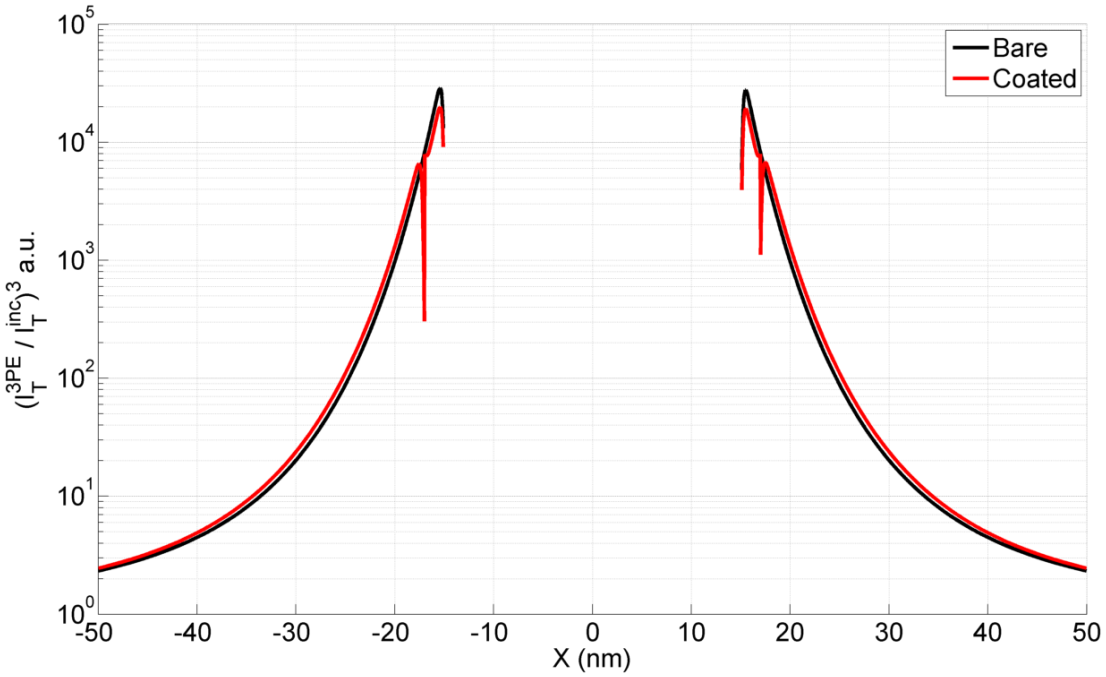

Figure S3 Third power of the total electromagnetic field intensity along the x-direction for (black curve) a bare gold NP and (red curve) a gold NP covered in molecules. The missing part in the plot corresponds to the region internal to the NP. The spikes around $|X| = 15$nm and 17nm are due to numerical instability produced by the discretization of the metal and coating surface, respectively.

In Figure S3 the spikes around $|X| = 15$nm and 17nm are ascribable to numerical inaccuracy near the discontinuity surfaces (metal/shell and shell/matrix). As we expect, the slope of the curves does not change remarkably between outside the NP and inside the coating because of the slight difference between the refractive index of the peptide ($n_p = 1.4$) and the water ($n_w = 1.33$). We can thus conclude that, for a first stage investigation of the electromagnetic field close to the NP surface, the molecules can be neglected.

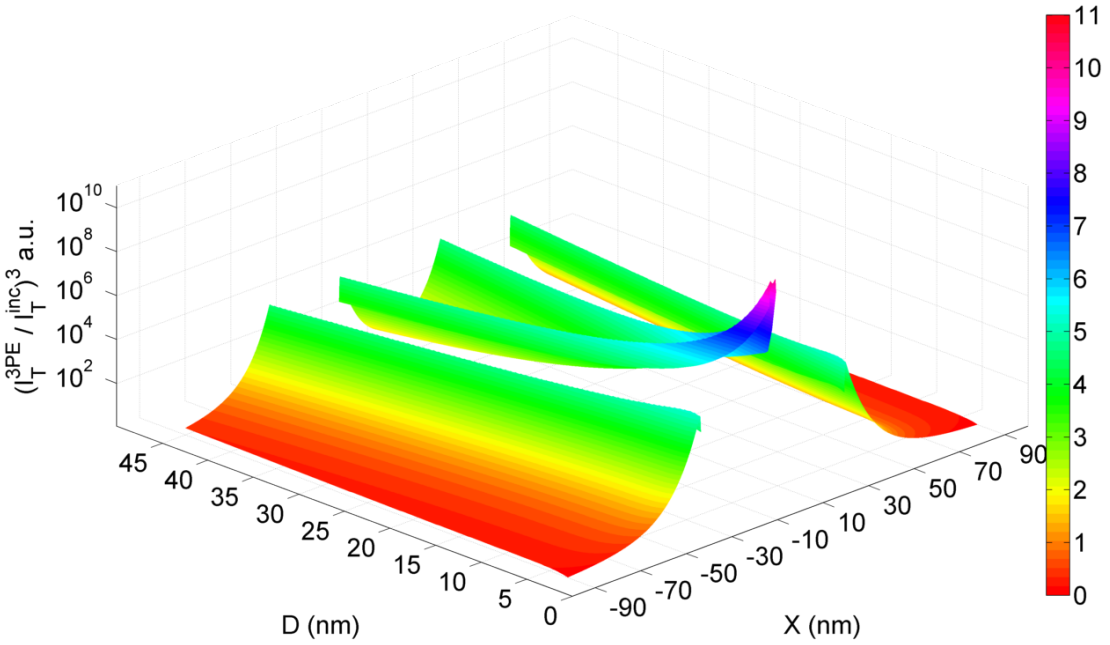

Figure S4 Third power of the total electromagnetic field intensity of a dimer along the x-direction for varying nanoparticle distances. The missing parts in the plots correspond to the regions internal to the NPs.

Comparison with analytical benchmarks

To verify the reliability of our simulations we tried out the results obtained by the MNPBEM toolbox with a benchmark code. The latter is an in-house fortran implementation, extracted from the book by Bohren and Huffman [53], of the Mie theory [66]. Such a code works out a quasi-exact solution, because a truncated expansion is involved, of the Maxwell equations when a spherical NP impinged by a plane wave is concerned. For this reason we perform the test only for an isolated NP.

The comparison between the electromagnetic field intensity averaged in time and space, Figure S5a, and only in time, Figure S5b, shows no difference between the pictured curves. Note that the slight intensity decreases close to the nanoparticle surface revealed by the BEM calculations are actually due to surface discretization effects. Thus, we can conclude that the MNPBEM toolbox and the in-house code lead to identical outcomes. As a result, we eventually claim that the toolbox by Hohenester and Trügler [50] provides reliable numerical solutions.

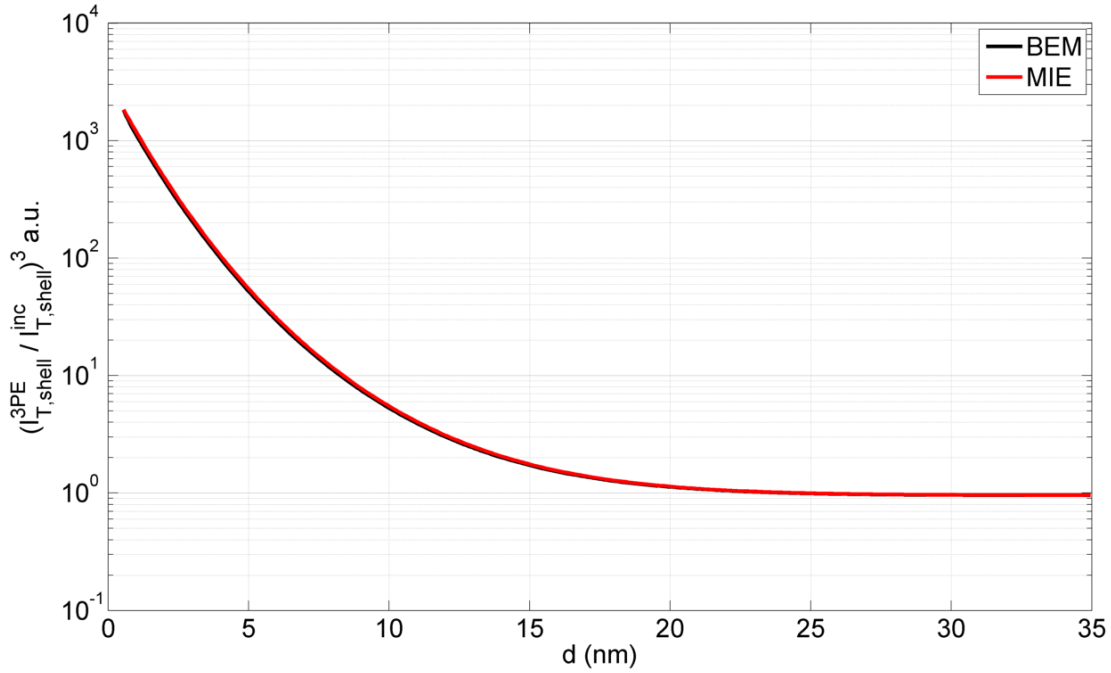

(a)

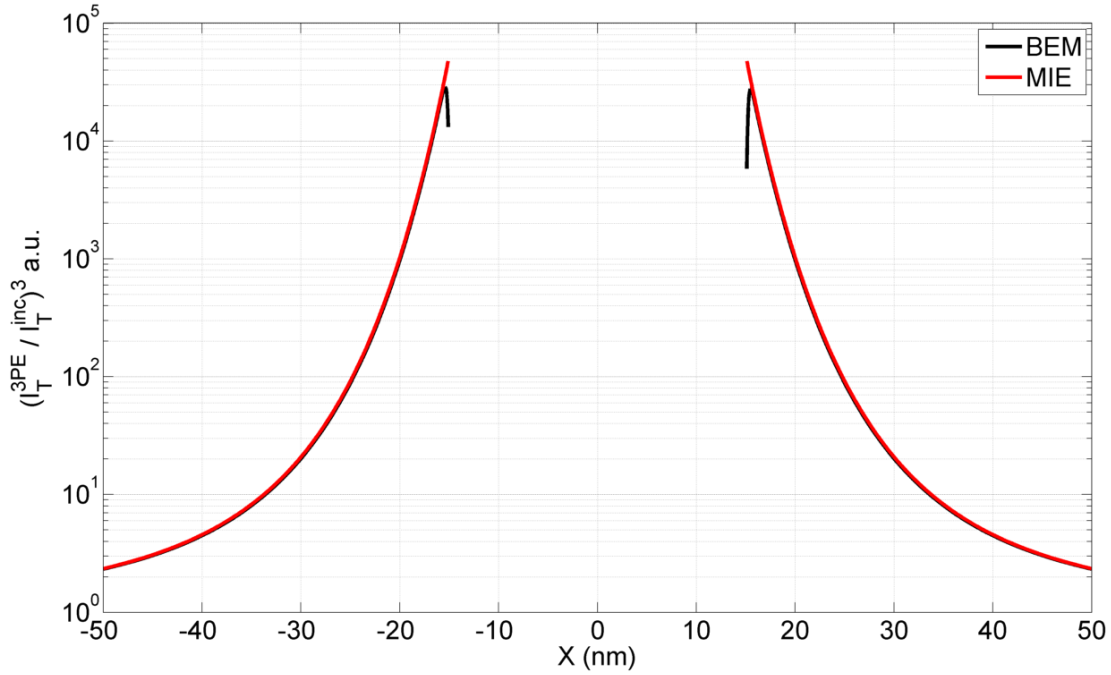

(b)

Figure S5 (a) Third power of the shell- and time-averaged total electromagnetic field intensity as a function of the distance from the NP surface (d). (b) Third power of the total electromagnetic field intensity along the x-direction. The missing part in the plot corresponds to the region internal to the NP. In both plots the "BEM" curve refers to the MNPBEM toolbox output, whereas the "MIE" one represents the outcomes obtained by the in-house Fortran implementation of the Mie theory.

Retarded vs. Quasi-Static

In principle, since the total size of the investigated systems in the radiation direction (at most about 80nm in the three particle triangular arrangement) is much smaller than the incident wavelength (561nm), the quasi-static approximation should provide reliable results. However, as shown in Ref.[39], even for 30nm gold NPs in water the quasi-static approach validity is dubious, so that we decided to exploit the safer retarded simulations. In this Section we check the validity of non-retarded calculations in predicting the optical behavior of isolated NPs and aggregates of NPs.

Figure S6a and S6b show that both the frameworks lead to very similar values of $(I_T^{3PE}/I_T^{inc})^3$. Indeed, the pictured curves reproduce the electromagnetic field intensities with the same order of magnitude when both single and coupled NPs are investigated. Thus, we can state that the predicted electric field enhancement around the NPs is the same. Note that the slight decrease close to the NP surface (missing parts in the plots) is caused by the surface discretization.

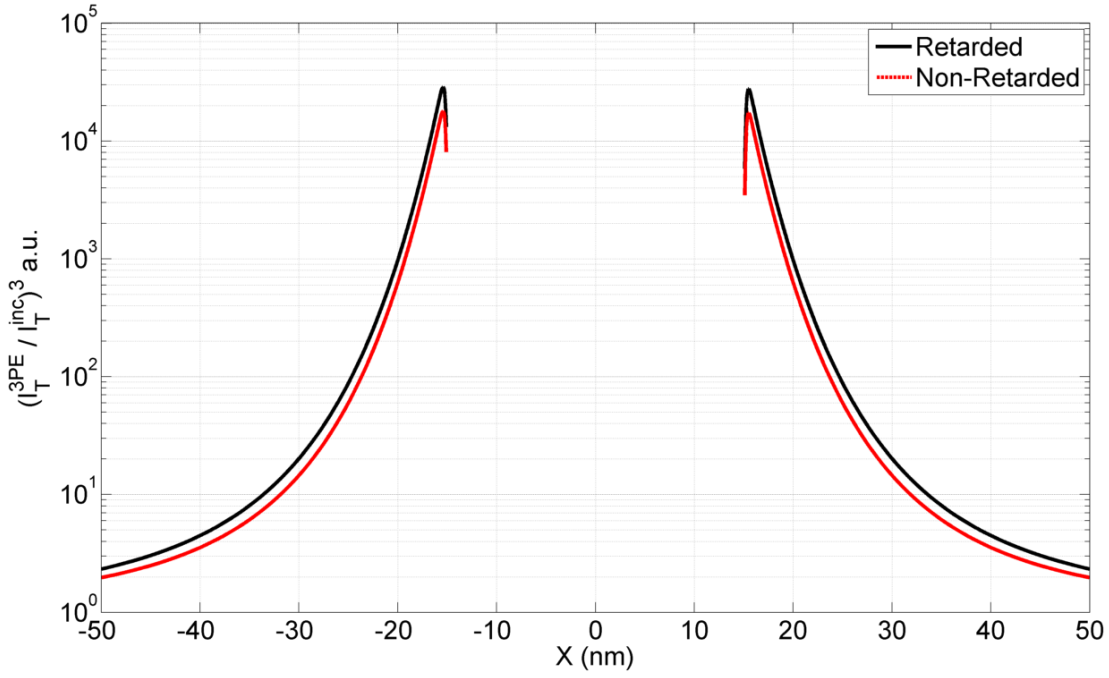

(a)

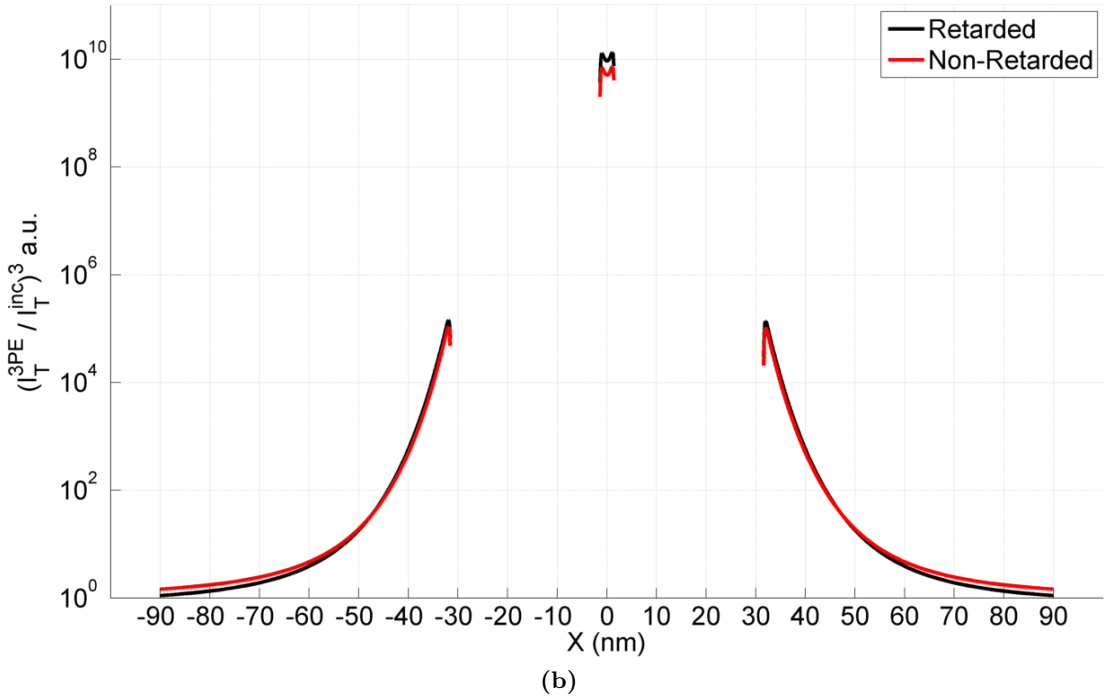

(b)

Figure S6 (a) Third power of the total electromagnetic field intensity along the x-direction for a bare gold NP. (b) Total electromagnetic field intensity to the third along the x-direction for a dimer of gold NPs. Calculations are performed with a surface separation between NPs of $D = 3$nm. In both plots the missing parts in the plots correspond to the regions internal to the NPs.

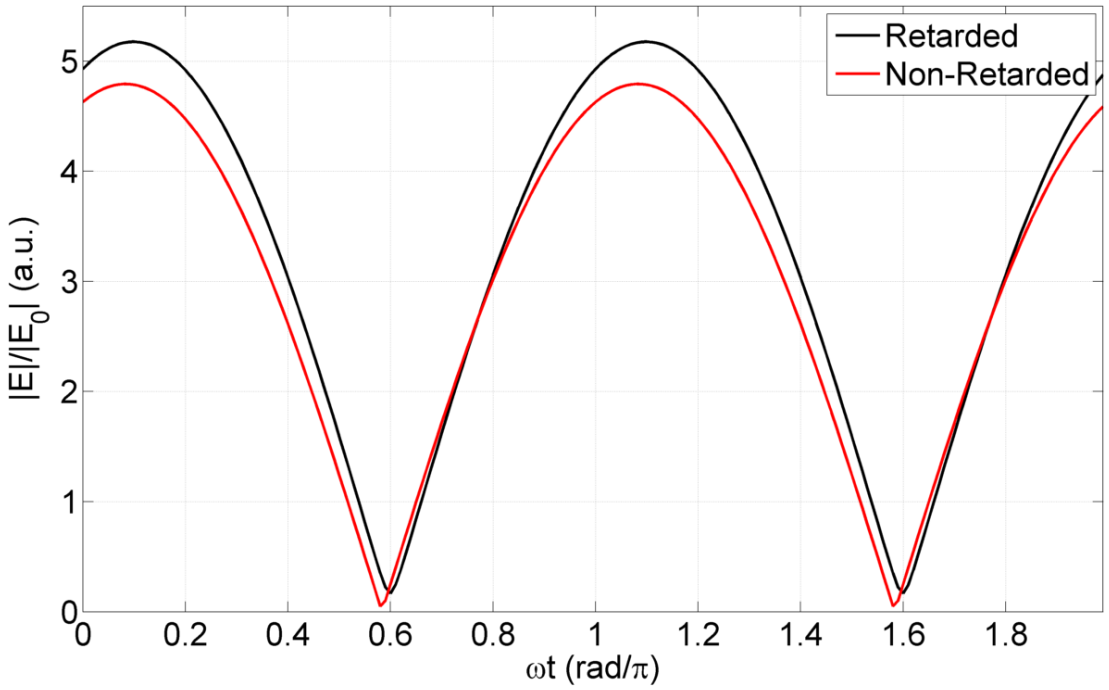

(a)

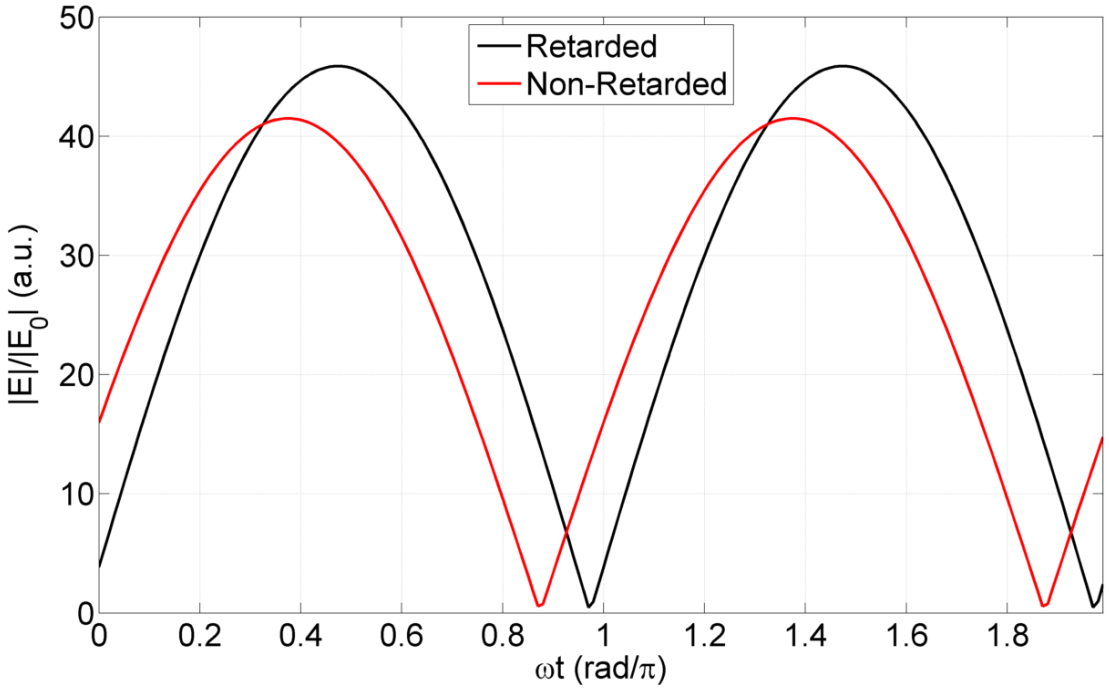

(b)

Figure S7 (a) Total electromagnetic field module as a function of time (t) in a point close to the NP surface along the x-axis. The calculations refer to an isolated NP. (b) Total electromagnetic field module as a function of time (t) in the middle point along the x-axis between two NPs. The calculations refer to coupled NPs separated from each other by $D = 3$nm. In both plots the symbol ω represents the incident radiation frequency.

In contrast, the dephasing occurring between the incident electromagnetic field and the plasmon field (i.e. the EM field revealing the greatest enhanced values) can vary

remarkably according to the selected approach. To study the plasmon dephasing, we calculate the electric field module as a function of time in specific points of both an isolated and a coupled NPs system. Figure S7a shows the results for a point along the x-axis close to the surface of an isolated NP. The abscissa represents the plasmon dephasing, which corresponds to a time delay (of the plasmon with respect to the incident radiation) equal to $0.05T$ and $0.04T$ for the retarded and non-retarded case, respectively (with T being the radiation period). If we focus on the middle point along the x-axis between coupled NPs (Figure S7b), the plasmon time delay reads $0.24T$ and $0.19T$ for the retarded and non-retarded case, respectively. Apart from the fact that the dephasing is greater for interacting NPs, it is clear that the difference between the two frameworks can be significant depending on the system under investigation. Hence, when the dephasing is an important parameter in an investigation, the use of the retarded theory becomes mandatory. In the presented study, since we are interested in time-averaged quantities, this difference does not affect the final results.

Test over the tessera number

To verify the validity of the chosen surface discretization for the nanoparticle/s, we carried out some simulations changing the number of select tesserae. For a spherical nanoparticle the maximum permitted number of pieces with equilateral triangular shape in which the sphere surface can be divided is 2884 in the MNPBEM toolbox: all the results presented in this work are obtained with this discretization. For the reliability of our results to be tested, we repeated some simulations keeping all the parameters fixed but the discretization, namely employing either 2044 or 1678 tesserae. All these three discretizations (2884, 2044 and 1678) correspond to three different amounts of triangular vertices commensurate to the surface of a sphere (i.e. 1444, 1024 and 841, respectively). Figures S8a and S8b show the trend of the ratio $(I_T^{3PE}/I_T^{inc})^3$ along the electric field incident direction (x-axis) outside an isolated NP and a couple of NPs separated by an intervening distance of 3nm, respectively. Both cases reveal an excellent agreement between the three curves obtained by different discretizations, leading us to conclude that 2884 is a reasonable number of tesserae for credible simulations.

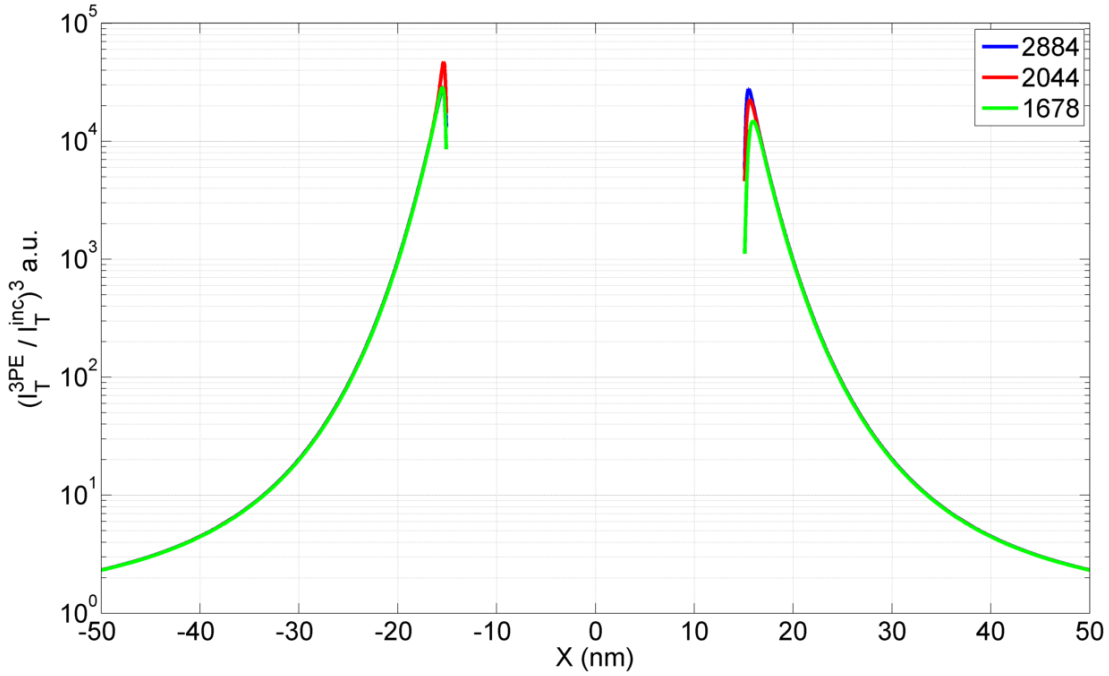

(a)

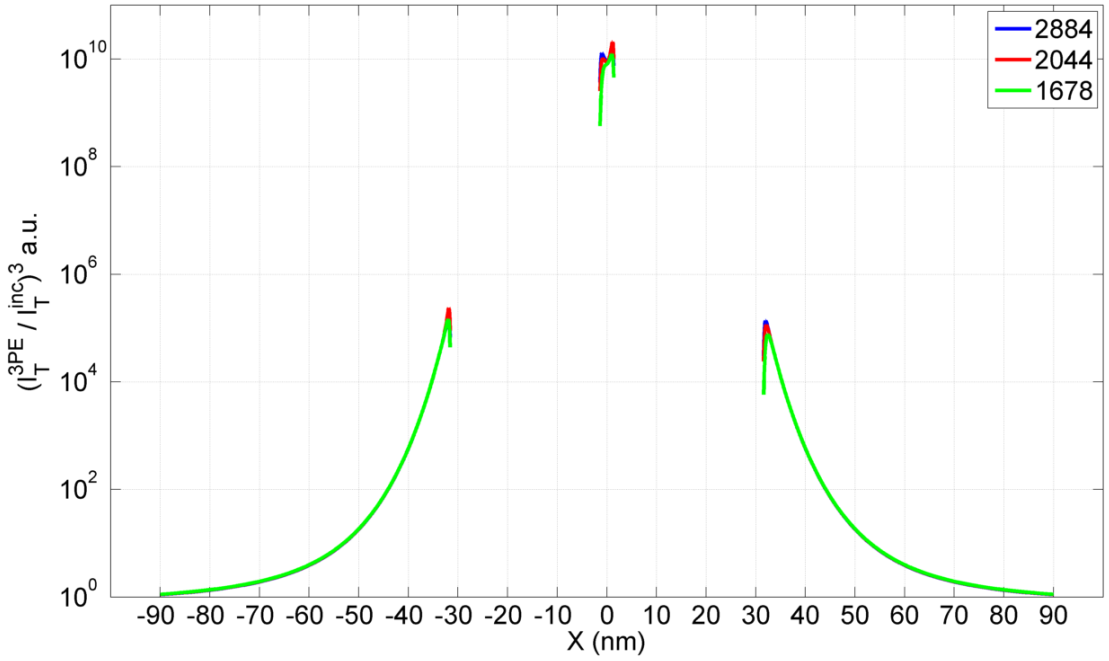

(b)

Figure S8 (a) Third power of the total electromagnetic field intensity along the direction of the incident electric field for an isolated sphere. (b) Third power of the total electromagnetic field intensity along the direction of the incident electric field for two spheres separated by 3nm between the surfaces. In both plots calculations are performed using three different amounts of tesserae reported in the legends. The missing parts in the plots correspond to the regions internal to the NPs.

Aggregate configurations

The dephasing of the NPs inside the two aggregates presented in the main text (Figure 11) is showed in Figure S9. The other configurations used to estimate the difference in electromagnetic field enhancement between the isolated dimer and the dimer embedded in an aggregate are displayed in Figures S10-S17. A table (Table 2) is also reported in the main text which summarizes the values of the polarization enhancement of the selected dimer when embedded in an aggregate composed of about 50 nanoparticles with respect to when the dimer is isolated.

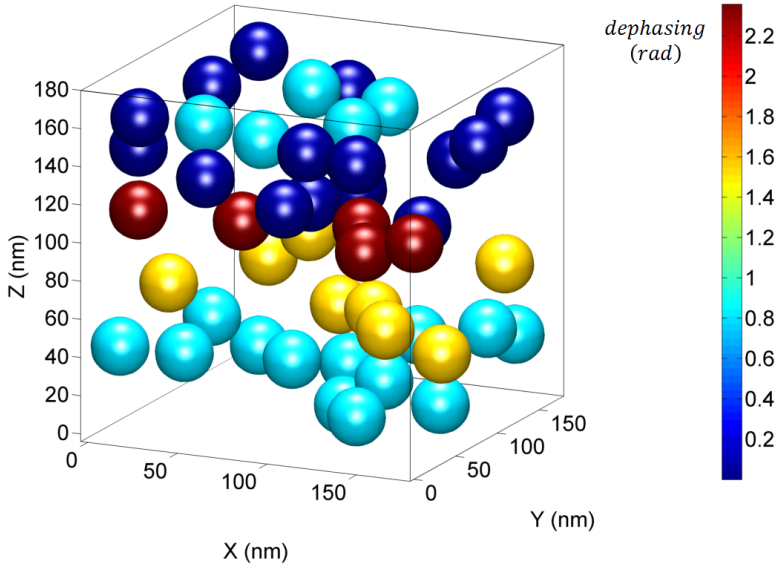

(a)

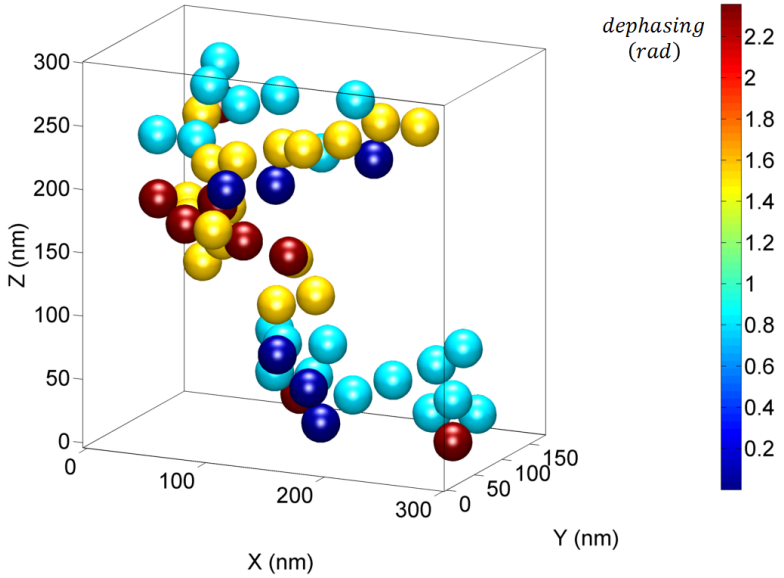

(b)

Figure S9 Results referring to the compact aggregate 1 and elongate aggregate 1 shown in the main text. Picture of the relative dephasing between the nanoparticles composing (a) a compact and (b) an elongate aggregate; the colorscale is in radiant units. The aggregates displayed here refer to the ones showed in Figure 11 in the main text.

Compact aggregate 2

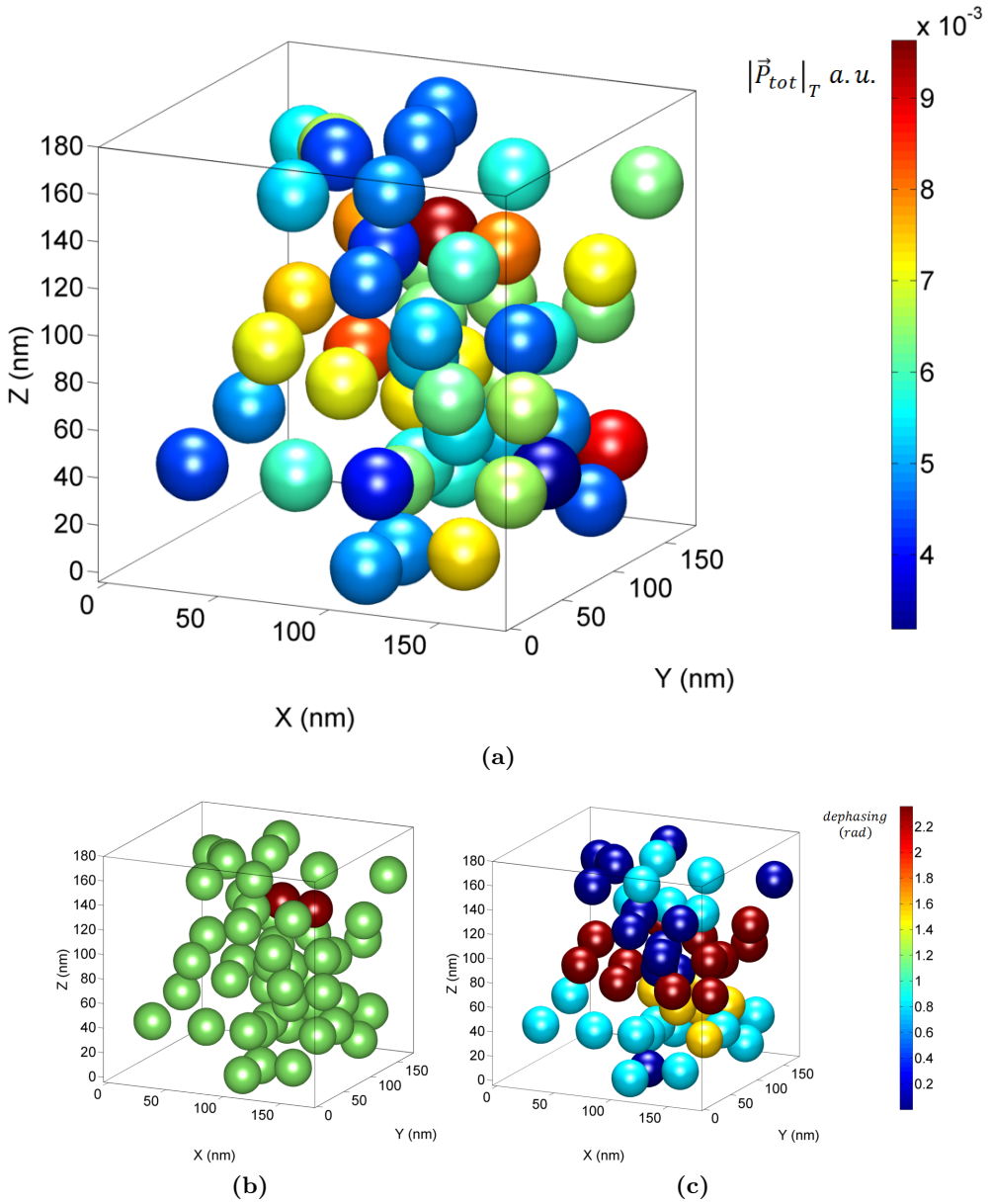

Figure S10 Results for compact aggregate 2. (a) Polarization module averaged in time of the nanoparticles composing the aggregate; the colorscale is in arbitrary units. (b) Sketch of the aggregate marking off (red nanoparticles) the dimer configuration selected inside the aggregate (green nanoparticles). (c) Picture of the relative dephasing between the nanoparticles of the aggregate; the colorscale is in radiant units.

Compact aggregate 3

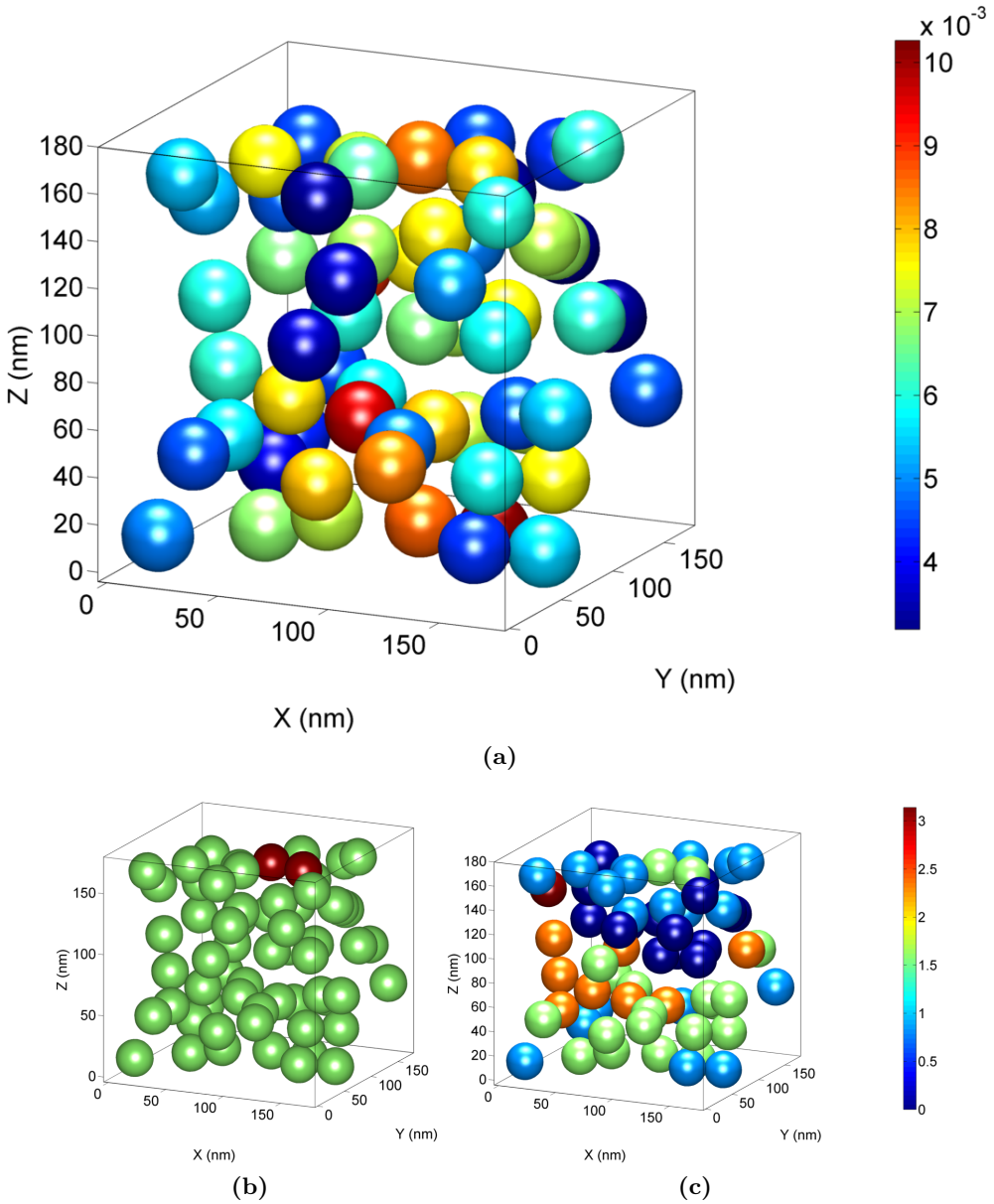

Figure S11 Results for compact aggregate 3. (a) Polarization module averaged in time of the nanoparticles composing the aggregate; the colorscale is in arbitrary units. (b) Sketch of the aggregate marking off (red nanoparticles) the dimer configuration selected inside the aggregate (green nanoparticles). (c) Picture of the relative dephasing between the nanoparticles of the aggregate; the colorscale is in radiant units.

Compact aggregate 4

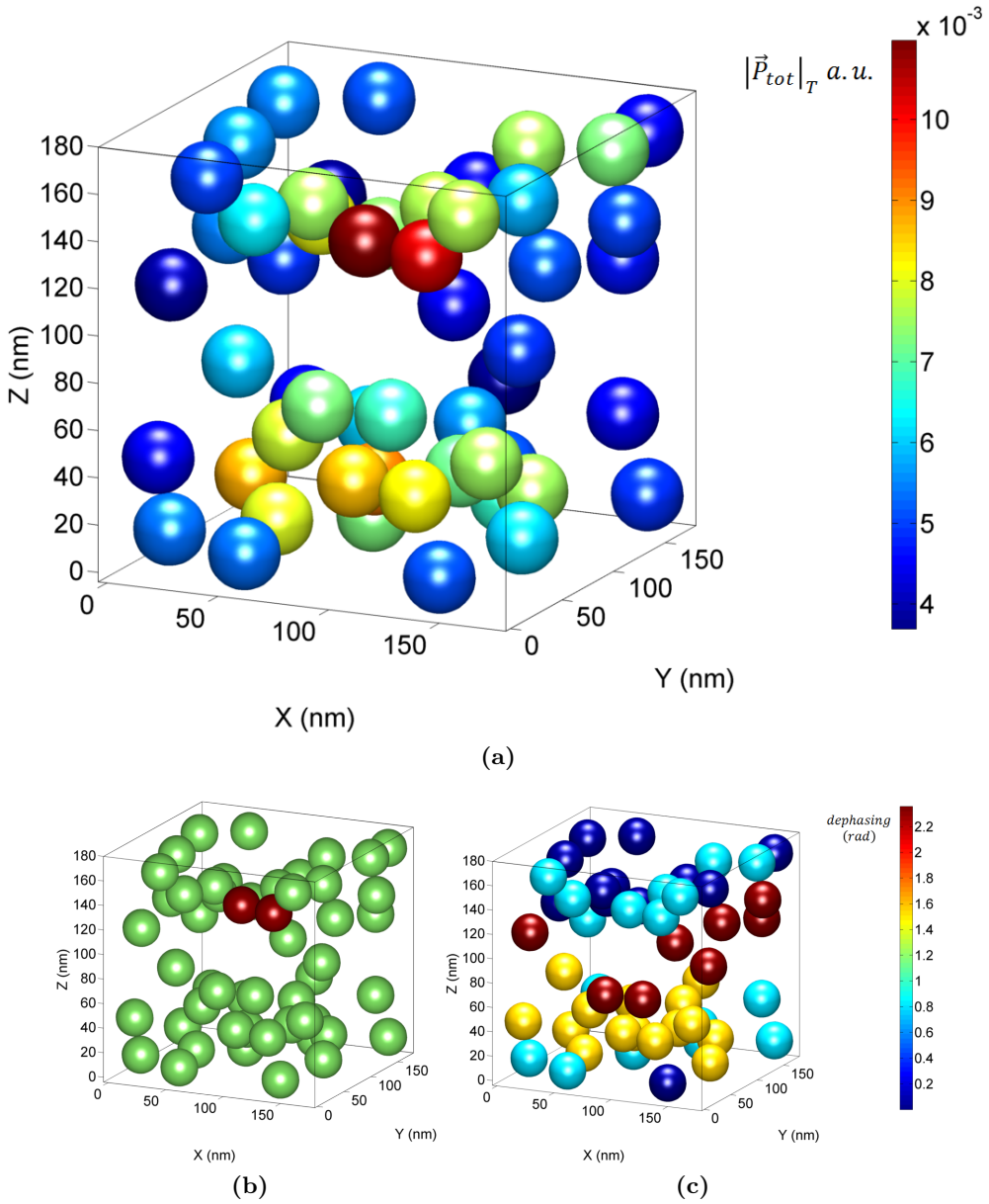

Figure S12 Results for compact aggregate 4. (a) Polarization module averaged in time of the nanoparticles composing the aggregate; the colorscale is in arbitrary units. (b) Sketch of the aggregate marking off (red nanoparticles) the dimer configuration selected inside the aggregate (green nanoparticles). (c) Picture of the relative dephasing between the nanoparticles of the aggregate; the colorscale is in radiant units.

Compact aggregate 5

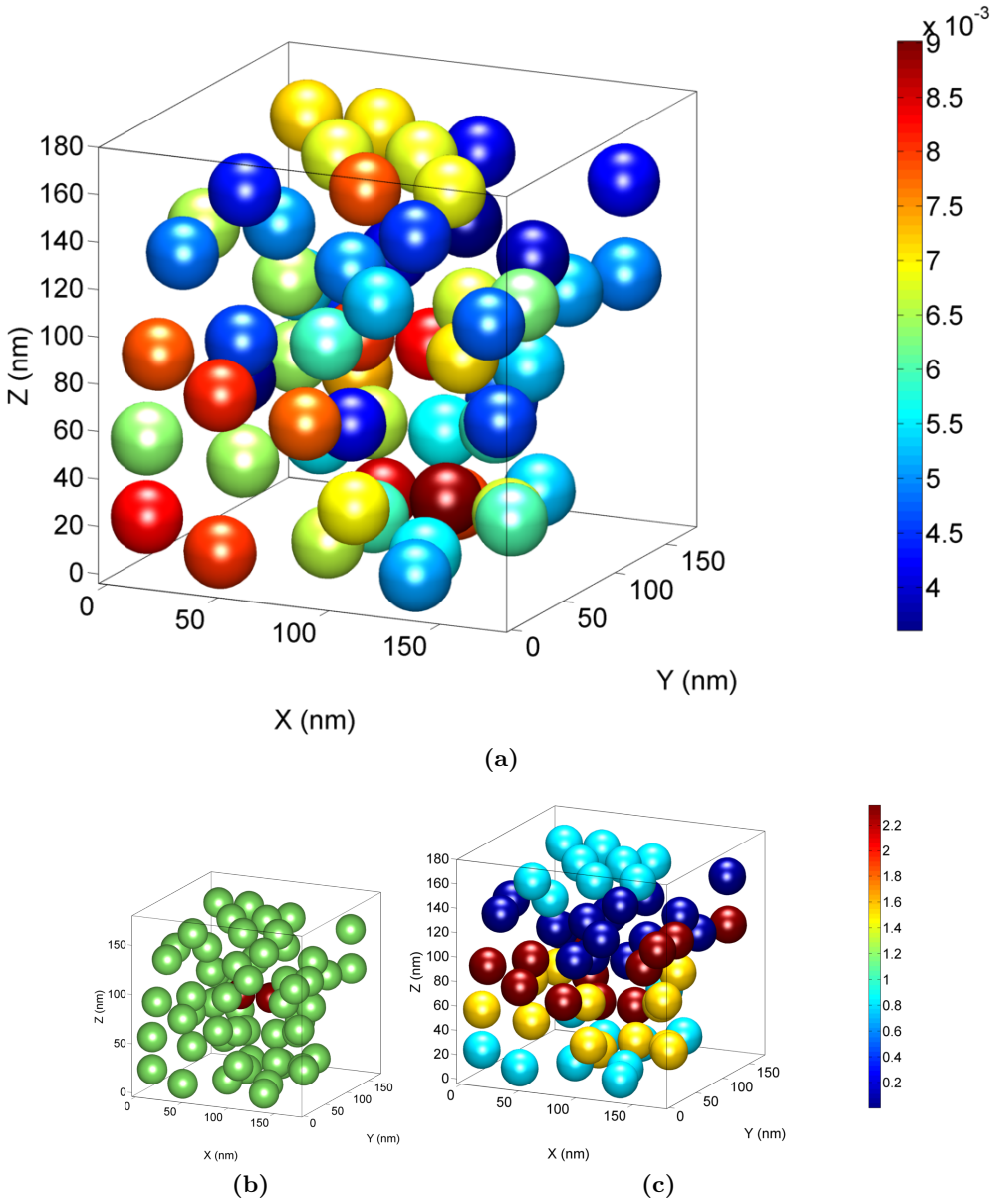

Figure S13 Results for compact aggregate 5. (a) Polarization module averaged in time of the nanoparticles composing the aggregate; the colorscale is in arbitrary units. (b) Sketch of the aggregate marking off (red nanoparticles) the dimer configuration selected inside the aggregate (green nanoparticles). (c) Picture of the relative dephasing between the nanoparticles of the aggregate; the colorscale is in radiant units.

Elongate aggregate 2

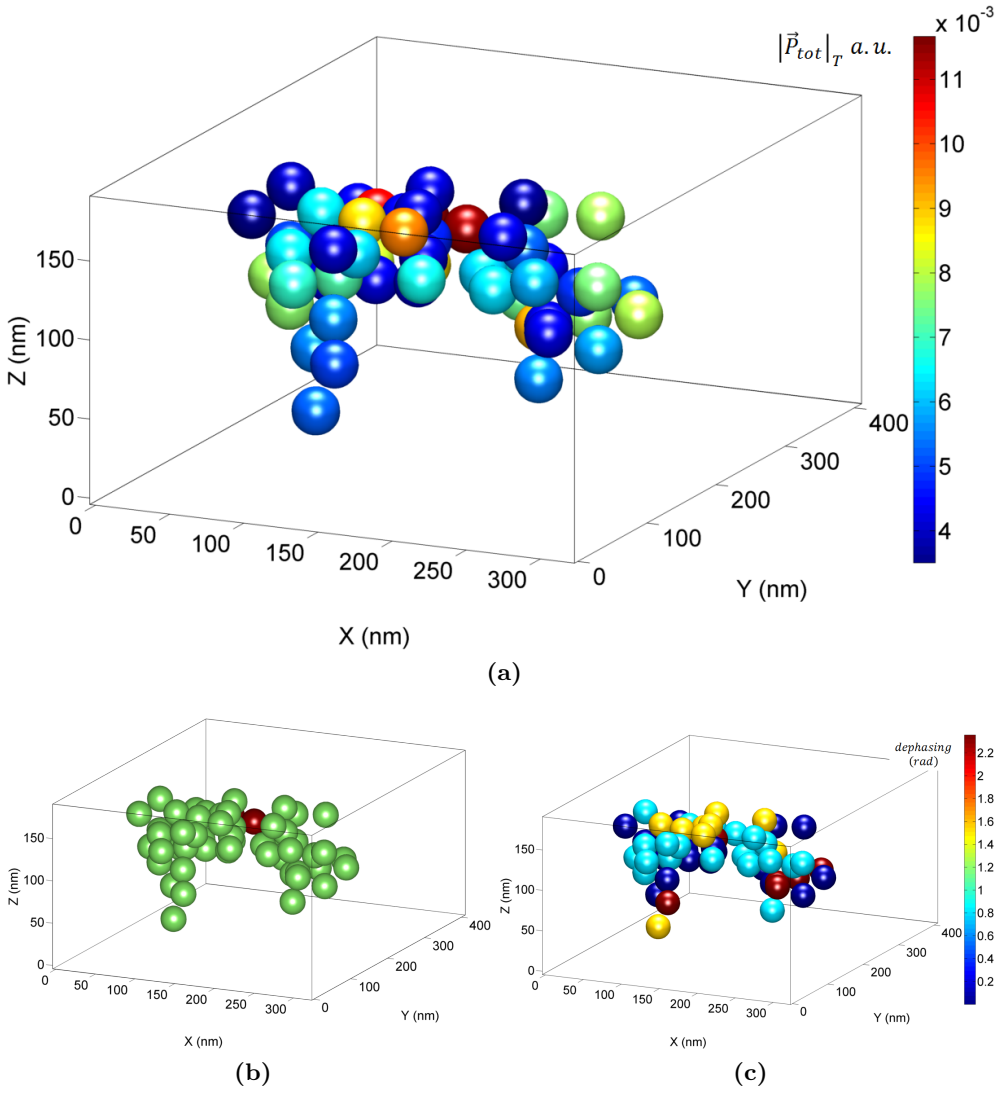

Figure S14 Results for elongate aggregate 2. (a) Polarization module averaged in time of the nanoparticles composing the aggregate; the colorscale is in arbitrary units. (b) Sketch of the aggregate marking off (red nanoparticles) the dimer configuration selected inside the aggregate (green nanoparticles). (c) Picture of the relative dephasing between the nanoparticles of the aggregate; the colorscale is in radiant units.

Elongate aggregate 3

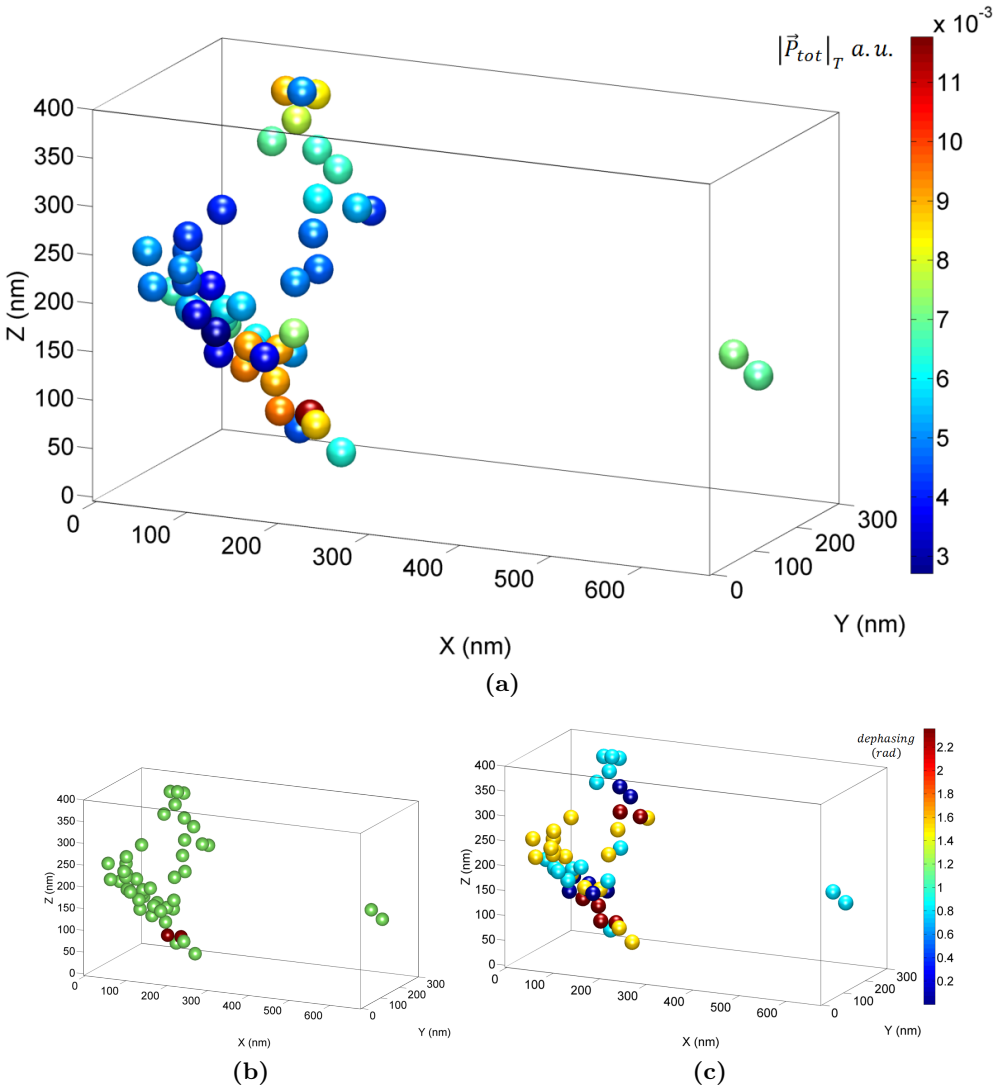

Figure S15 Results for elongate aggregate 3. (a) Polarization module averaged in time of the nanoparticles composing the aggregate; the colorscale is in arbitrary units. (b) Sketch of the aggregate marking off (red nanoparticles) the dimer configuration selected inside the aggregate (green nanoparticles). (c) Picture of the relative dephasing between the nanoparticles of the aggregate; the colorscale is in radiant units.

Elongate aggregate 4

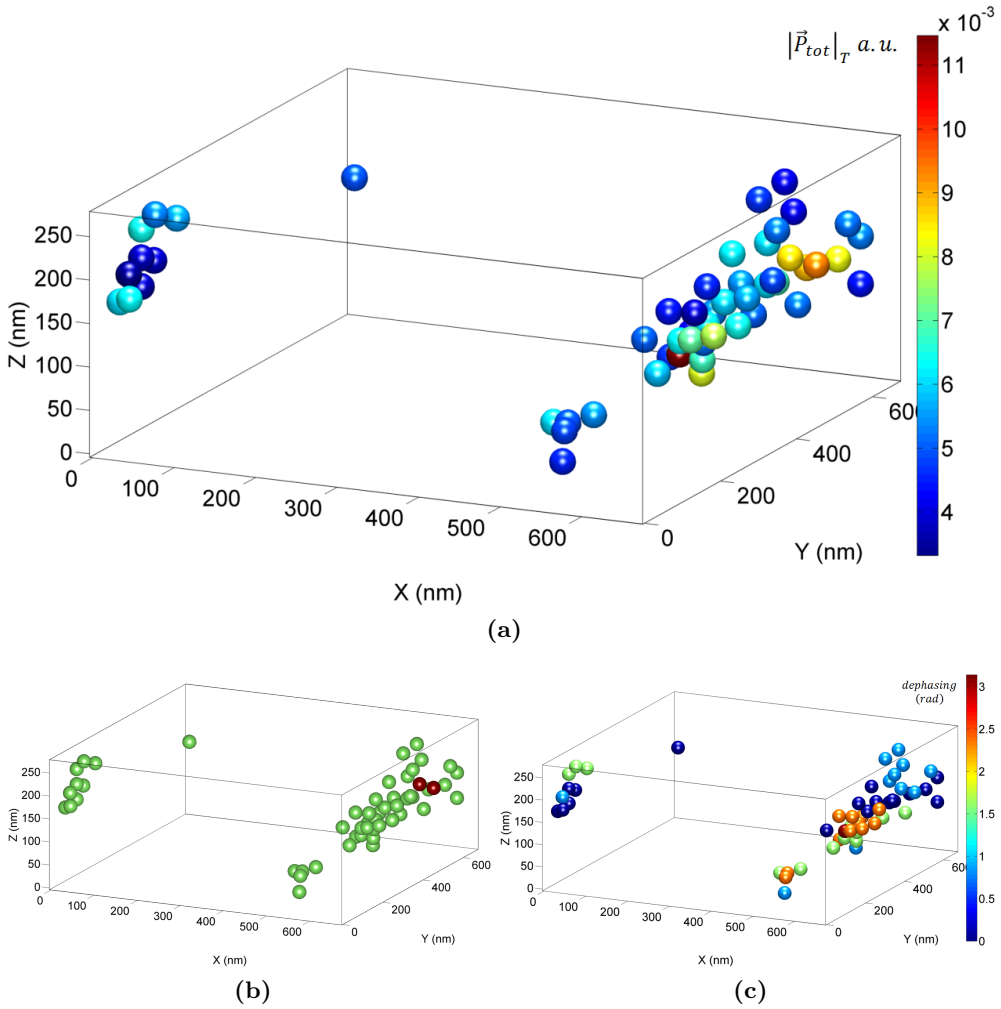

Figure S16 Results for elongate aggregate 4. (a) Polarization module averaged in time of the nanoparticles composing the aggregate; the colorscale is in arbitrary units. (b) Sketch of the aggregate marking off (red nanoparticles) the dimer configuration selected inside the aggregate (green nanoparticles). (c) Picture of the relative dephasing between the nanoparticles of the aggregate; the colorscale is in radiant units.

Elongate aggregate 5

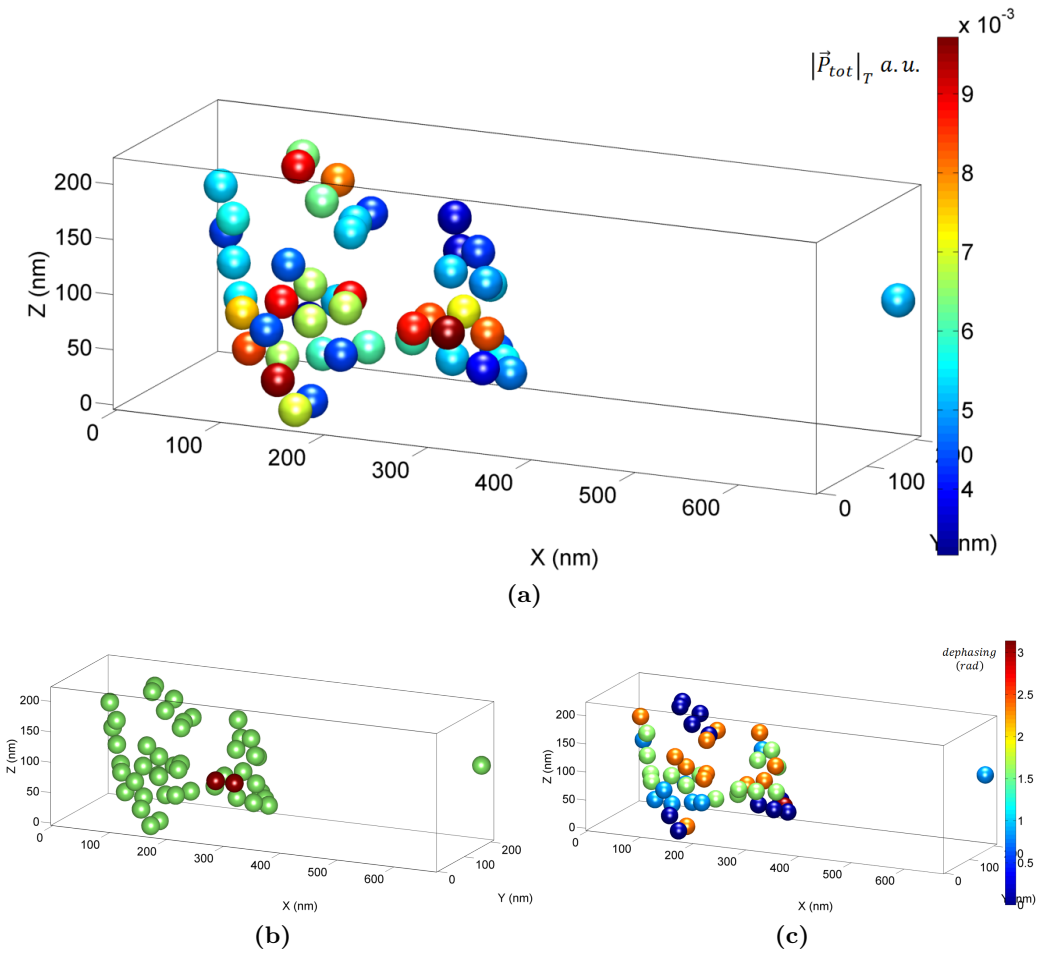

Figure S17 Results for elongate aggregate 5. (a) Polarization module averaged in time of the nanoparticles composing the aggregate; the colorscale is in arbitrary units. (b) Sketch of the aggregate marking off (red nanoparticles) the dimer configuration selected inside the aggregate (green nanoparticles). (c) Picture of the relative dephasing between the nanoparticles of the aggregate; the colorscale is in radiant units.